



**HAL**  
open science

## Drug-Loaded Lipid-Coated Hybrid Organic-Inorganic “Stealth” Nanoparticles for Cancer Therapy

Xue Li, Giuseppina Salzano, Jingwen Qiu, Mathilde Ménard, Kristian Berg,  
Theodossis Theodossiou, Catherine Ladavière, Ruxandra Gref

► **To cite this version:**

Xue Li, Giuseppina Salzano, Jingwen Qiu, Mathilde Ménard, Kristian Berg, et al.. Drug-Loaded Lipid-Coated Hybrid Organic-Inorganic “Stealth” Nanoparticles for Cancer Therapy. *Frontiers in Bioengineering and Biotechnology*, 2020, 8, 10.3389/fbioe.2020.01027 . hal-02917638v1

**HAL Id: hal-02917638**

**<https://cnrs.hal.science/hal-02917638v1>**

Submitted on 5 Jan 2021 (v1), last revised 18 Oct 2022 (v2)

**HAL** is a multi-disciplinary open access archive for the deposit and dissemination of scientific research documents, whether they are published or not. The documents may come from teaching and research institutions in France or abroad, or from public or private research centers.

L'archive ouverte pluridisciplinaire **HAL**, est destinée au dépôt et à la diffusion de documents scientifiques de niveau recherche, publiés ou non, émanant des établissements d'enseignement et de recherche français ou étrangers, des laboratoires publics ou privés.

# 1 **Drug-loaded lipid-coated hybrid organic-inorganic “stealth”** 2 **nanoparticles for cancer therapy**

3 **Xue Li<sup>1</sup>, Giuseppina Salzano<sup>1</sup>, Jingwen Qiu<sup>1</sup>, Mathilde Menard<sup>2</sup>, Kristian Berg<sup>2</sup>, Theodossis**  
4 **Theodossiou<sup>2</sup>, Catherine Ladavière<sup>3</sup>, Ruxandra Gref<sup>1\*</sup>**

5 <sup>1</sup> Université Paris-Saclay, CNRS UMR 8214, Institut des Sciences Moléculaires d'Orsay, 91405, Orsay,  
6 France.

7 <sup>2</sup> Department of Radiation Biology, Institute for Cancer Research, Norwegian Radium Hospital, Oslo  
8 University Hospital, 0372, Oslo, Norway.

9 <sup>3</sup> University of Lyon, CNRS, UMR 5223, IMP, 15 bd André Latarjet, F-69622, Villeurbanne, France

## 10 **\* Correspondence:**

11 Ruxandra Gref

12 ruxandra.gref@universite-paris-saclay.fr

13 **Keywords: metal organic frameworks, nanoparticles, lipids, poly(ethylene glycol), stealth,**  
14 **sustained drug release.**

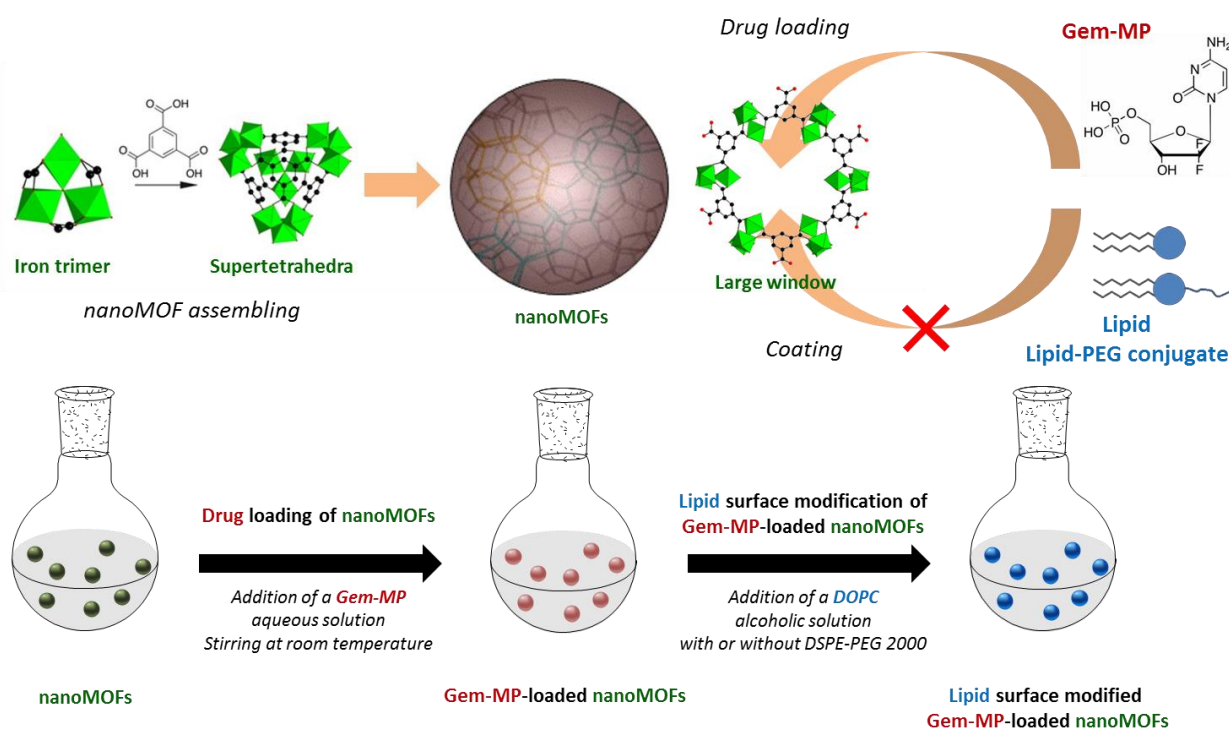
## 15 **Abstract**

16 Hybrid porous nanoscale metal organic frameworks (nanoMOFs) made of iron trimesate are attracting  
17 increasing interest as drug carriers due to their high drug loading capacity, biodegradability, and  
18 biocompatibility. NanoMOF surface modification to prevent clearance by the innate immune system  
19 remains still challenging in reason of their high porosity and biodegradable character. Herein, FDA-  
20 approved lipids and poly(ethylene glycol) (PEG)-lipid conjugates were used to engineer the surface of  
21 nanoMOFs by a rapid and convenient solvent-exchange deposition method. The resulting lipid-coated  
22 nanoMOFs were extensively characterized. For the first time, we show that nanoMOF surface  
23 modification with lipids affords a better control over drug release and their degradation in biological  
24 media. Moreover, when loaded with the anticancer drug Gem-MP (Gemcitabine-monophosphate), iron  
25 trimesate nanoMOFs acted as “Trojan horses” carrying the drug inside cancer cells to eradicate them.  
26 Moreover, the PEG-coated nanoMOFs escaped the capture by macrophages. In a nutshell, versatile  
27 PEG-based lipid shells control cell interactions and open perspectives for drug targeting.

## 28 **Introduction**

29 Despite progresses in drug development and cancer biology, cancer mortality rate remains over 30%,  
30 and the morbidity much higher. Nanomedicine has shown great promise through drug delivery by  
31 achieving drug transcytosis, drug targeting and theranostics (Rosenblum et al., 2018; Senapati et al.,  
32 2018). Nanoscale metal organic frameworks (nanoMOFs) recently emerged as an attracting class of  
33 hybrid nanomaterials for biomedical applications due to their biodegradability, biocompatibility,  
34 elevated drug loading capacity and high versatility in terms of architecture and physico-chemical  
35 properties (Horcajada et al., 2010, 2012; He et al., 2015; Rojas et al., 2019). NanoMOFs are formed  
36 by the self-assembly of metal centers and organic ligands, leading to the formation of open crystalline  
37 structures with regular and high porosities. Particularly, nanoMOFs based on iron (III) trimesate are  
38 among the most widely studied (Figure 1 upper panel) (Horcajada et al., 2010; Agostoni et al., 2013;  
39 Baati et al., 2013; Simon-Yarza et al., 2016; Li et al., 2019a). Recently, they were shown to display

40 several intrinsic properties of main interest in the nanomedicine field: radio-enhancement properties  
 41 when submitted to  $\gamma$ -irradiation (Li et al., 2019a); they behaved as T<sub>2</sub>-weighted MRI imaging contrast  
 42 agents (Horcajada et al., 2010) and they had intrinsic antibacterial effects killing intracellular bacteria  
 43 (Li et al., 2019b).



44

45 **Figure 1. Upper panel.** Schematic representation of the MIL-100(Fe) nanoMOF assembly from iron  
 46 trimers and trimesic acid. Gem-MP was loaded by impregnation from aqueous solutions, penetrating  
 47 inside the nanoMOFs through their largest windows (approx. 9 Å in size). Lipid molecules (DOPC and  
 48 DSPE-PEG 2000) with larger molecular dimensions than the large windows were used to coat the  
 49 nanoMOFs. **Lower panel.** Preparation steps of lipid-coated nanoMOFs. First, Gem-MP was loaded,  
 50 into the nanoMOFs followed by their coating with lipid shells and PEG-lipid conjugates.

51 In addition, iron trimesate nanoMOFs MIL-100 (Fe) (MIL stands for Material from Institut Lavoisier)  
 52 exhibited high drug loading capacity soaking a variety of drugs from their aqueous solutions with yields  
 53 close to 100%. In the case of Gemcitabine-monophosphate (Gem-MP), the drug payload reached ~30  
 54 wt% with >98% drug loading efficiency (Rodriguez-Ruiz et al., 2015). Gem-MP, the active  
 55 intermediate of Gem, is widely used in various carcinomas, including pancreatic cancer, bladder  
 56 cancer, and non-small cell lung cancer. The administration of Gem-MP is of high interest for resistant  
 57 cancer treatment since the phosphorylation of Gem can be a rate-limiting step especially difficult for  
 58 resistant cancer cells. However, Gem-MP administration is hampered by its poor stability in biological  
 59 media and low cellular uptake (Bouffard et al., 1993). In this challenging context, some of us showed  
 60 that Gem-MP could be protected against degradation with increased cellular uptake by encapsulation  
 61 in nanoMOFs (Rodriguez-Ruiz et al., 2015).

62 Surface modifications are essential to control drug release and modulate the *in vivo* fate of nanoMOFs  
 63 in the living body. Silica coatings were employed in an attempt to control the release of loaded  
 64 molecules from nanoMOFs MIL-101 (Taylor-Pashow et al., 2009). NanoMOFs were coated with lipid  
 65 bilayers to improve their uptake by cancer cells (Wuttke et al., 2015) or with chitosan to increase their

66 intestinal permeability (Hidalgo et al., 2017). Heparin coatings endowed the nanoMOFs with longer-  
67 blood circulation time (Bellido et al., 2015).

68 Poly(ethylene glycol) (PEG) based materials remain the most employed ones to engineer coatings able  
69 to prevent nanoparticles (NPs) clearance by the innate immune system, which is a prerequisite for  
70 biomedical applications (Gref et al., 1994, 1995). However, as compared to dense polymeric NPs, the  
71 porous nanoMOFs are more challenging to be coated with PEG, because these linear chains readily  
72 penetrate within their porosity, inducing an uncontrolled “burst” drug release (Agostoni et al., 2015).  
73 There are still scarce examples of successful PEGylated nanoMOF formulations. PEG was crosslinked  
74 onto the nanoMOF’s surface to avoid its penetration inside the porous cores (Giménez-marqués et al.,  
75 2018) but resulted in a non-biodegradable coating. Alternatively, nanoMOFs were coated with  
76 inclusion complexes consisting of functionalized cyclodextrins (CDs) and PEG chains coupled to  
77 adamantane (Agostoni et al., 2015; Aykac et al., 2017; Cutrone et al., 2019a). Finally, comb-like  
78 copolymers consisting of polysaccharides grafted with moieties able to coordinate to the nanoMOFs  
79 and PEG chains were synthesized and anchored onto the nanoMOFs (Cutrone et al., 2019b). However,  
80 all these coatings imply sophisticated chemistry strategies and/or several preparation steps, which  
81 might restrict their further applications. Moreover, all the PEGylated (macro) molecules used in the  
82 previous studies are not approved by Food and Drug Administration (FDA).

83 In this context, we propose to engineer for the first time PEGylated coatings on nanoMOFs by using  
84 only FDA-approved materials using a convenient one-step method. To date, Doxil® and Onivyde®  
85 represent the only FDA-approved PEGylated NPs (Barenholz, 2012), where DSPE-PEG 2000 (1,2-  
86 distearoyl-*sn*-glycero-3-phosphoethanolamine-N-[amino(polyethylene glycol)-2000] sodium salt)  
87 were used in both cases. Herein, DSPE-PEG 2000 was used in combination with DOPC (1,2-dioleoyl-  
88 *sn*-glycero-3-phosphocholine) to functionalize the surface of iron trimesate MOFs (Figure 1 lower  
89 panel). Moreover, we show that the PEG-based coating have an impact on both drug release and  
90 nanoMOFs degradation, which was not the case with the coatings used so far. Finally, the coatings  
91 were able not only to reduce macrophage uptake *in vitro* but also to eradicate cancer cells.

## 92 MATERIALS AND METHODS

### 93 Materials

94 Iron (III) chloride hexahydrate (98%) was purchased from Alfa Aesar (Schiltigheim, France). 1,3,5-  
95 benzenetricarboxylic acid (BTC, 95%) and absolute ethanol (99%) were from Sigma-Aldrich (Saint-  
96 Quentin-Fallavier, France). These materials were used for the synthesis of nanoMOFs. Amoxicillin  
97 (Amox) from Sigma-Aldrich (Saint-Quentin-Fallavier, France) and 2',2'-difluorodeoxycytidine  
98 monophosphate (Gem-MP) from Toronto Research Chemicals (North York, Canada) were the drugs  
99 used in this study. 1,2-dioleoyl-*sn*-glycero-3-phosphocholine (DOPC) and (1,2-distearoyl-*sn*-glycero-  
100 3-phosphoethanolamine-N-[amino(polyethylene glycol)-2000] sodium salt (DSPE-PEG 2000) were  
101 ordered from Avanti Polar Lipids (Alabama, United States) as coating materials. 3-(4,5-Dimethyl-2-  
102 thiazolyl)-2,5-diphenyl-2H-tetrazolium bromide (MTT, Sigma-Aldrich, Oslo, Norway) was used for  
103 toxicity evaluation of nanoMOFs. All the chemicals were used without further purification.

### 104 Cell culture

105 Murine macrophage cell line J774A.1, *CelluloNet biobank BB-0033-00072*, were grown in RPMI-1640  
106 medium (Thermo Fisher Scientific, Villebon-sur-Yvette, France) supplemented with 10% v/v  
107 decomplemented fetal bovine serum (FBS, Thermo Fisher Scientific, Villebon-sur-Yvette, France),  
108 1% L-Glutamine (Sigma-Aldrich, Oslo, Norway), and 1% (P/S, Sigma-Aldrich, Oslo, Norway) at

109 37°C in humidified air containing 5% CO<sub>2</sub>. SKOV3 ovarian cancer cell were cultivated in a RPMI-  
110 1640 media without phenol red supplemented with 10% FBS, 5% L-Glutamine and 5%  
111 penicillin/streptomycin (P/S) at 37°C in a 5% CO<sub>2</sub> humidified atmosphere.

## 112 **Synthesis and characterization of MIL-100(Fe) nanoMOFs**

113 Iron trimesate nanoMOFs was synthesized by microwave assisted hydrothermal reaction as previously  
114 described [6]. Briefly, 20 mL of aqueous mixture containing 6.0 mM of iron chloride hexahydrate and  
115 4.02 mM of trimesic acid (TA, 1,3,5-benzenetricarboxylic acid) was heated at 130 °C for 6 min under  
116 stirring. The reaction was carried out with the power of 1600 W (Mars-5, CEM, USA). The as-  
117 synthesized nanoMOFs were harvested by centrifugation (10,000 g, 15 min) and washed with absolute  
118 ethanol to remove the excessive TA until the supernatant became colorless. NanoMOFs were stored in  
119 ethanol at room temperature for further usage at the concentration of 18.2 mg/mL.

120 SEM images were acquired on a Zeiss SUPRA 55 VP field emission gun scanning electron microscope  
121 fitted with an EDAX EDS analytical system. It was set to a low voltage (1 kV) and low current (a few  
122 pA) in order not to damage the samples and to avoid any conductive coating that could bother direct  
123 observation of the samples. Secondary electron type detector was used to record the images.

124 Dynamic light scattering (DLS) measurements were performed at 25°C on a Malvern Zetasizer Nano-  
125 ZS instrument at 90° angle. The mean hydrodynamic diameter of the particles was determined in a  
126 diluted aqueous suspension at 50 µg/mL.

127 Nanoparticle tracking analysis (NTA) was performed on Malvern NanoSight (LM10 Instrument,  
128 Malvern Instruments Ltd, Orsay, France), which combines a conventional optical microscope with a  
129 laser to illuminate the NPs in Brownian motion. It is used to individually follow nanoMOFs to gain  
130 insight into their size distribution and concentration.

131 Zeta potential (ZP) of nanoMOFs were measured at 25°C using a Zetasizer Nano-ZS instrument at  
132 different pH ranging from 3 to 10. NanoMOFs was diluted to 100 µg/mL with 1mM KCl. Measured  
133 electrophoretic mobilities were converted to zeta potential values according to the Smoluchowski  
134 equation. Nitrogen sorption measurements were performed on a Micromeritics Instruments ASAP  
135 2020 at 77 K. Samples were degassed at 100 °C for 15 h. BET surface area was calculated in the partial  
136 pressure range of 0.05 – 0.20 P/P<sub>0</sub>.

## 137 **Drug encapsulation in nanoMOFs**

138 Drugs (Gem-MP and Amox) were loaded within nanoMOFs simply by impregnation of drug(s)  
139 aqueous solutions and nanoMOFs. Practically, nanoMOFs suspension (1.0 mg) were centrifuged for  
140 10 min at 10,000 g and re-suspended in 1 mL of aqueous drug solutions (0.125 ~ 1 mg/mL for Amox  
141 and 0.08 ~ 0.2 mg/mL for Gem-MP) or water as a control. Different drug concentrations were used to  
142 optimize the drug encapsulation. After incubation at room temperature under gentle stirring for several  
143 hours (12 h for Amox and 4 h for Gem-MP), the nanoMOFs were recovered by centrifugation at 10,000  
144 g for 10 min. The non-encapsulated drug in the supernatant was quantified by adapting previously  
145 described High Performance Liquid Chromatography (HPLC) methods (Li et al., 2019a, 2019b).  
146 Specifically, HPLC analysis was performed on an Agilent system using a tunable UV absorbance  
147 detector. The injection volume of AMOX was 10 µL followed by eluant flow at a rate of 0.5 mL/min  
148 through a C18 Silica column (4.6 × 250 mm, 5 µm; Phenomenex) maintained at 30°C. The mobile  
149 phase consisted of 30% (v/v) methanol containing 5.2 mg/mL of sodium dihydrogene phosphate  
150 monohydrate. The pH was adjusted to 5 using phosphoric acid solution. AMOX were detected at 247

151 nm and retention times were 4.6 minutes. Similarly, Gem-MP was detected using the same Agilent  
 152 system and column. The mobile phase was composed of 84% buffer (0.2 M (TEAA)): 16% methanol.  
 153 It was detected at 254 nm with an injection volume of 10  $\mu$ l. The drug payload was calculated as  
 154 Equation (1):

$$155 \quad \text{Payload (\%)} = \frac{\text{Encapsulated Drug (mg)}}{\text{nanoMOFs (mg)}} \times 100 \quad (1)$$

## 156 **Surface modification of nanoMOFs with DOPC lipids and PEG-lipid conjugates**

157 Surface modification was performed using a “green” method. To prepare DOPC coated nanoMOFs,  
 158 60  $\mu$ l of nanoMOFs was mixed with 40  $\mu$ l of DOPC alcoholic solution containing 100  $\mu$ g of DOPC.  
 159 Subsequently, 900  $\mu$ l of water was rapidly added using an electronic pipette. The weight ratio between  
 160 DOPC and nanoMOF was in the range of 1:20 ~ 1:1. In the case of PEG-lipid conjugates coated  
 161 nanoMOFs, 20 wt% of DOPC was replaced by DSPE-PEG 2000.

## 162 **Characterization of lipid coated nanoMOFs**

### 163 **Lipid quantification**

164 DOPC quantification was performed by using a colorimetric enzymatic method (BIOLABO, Maizy,  
 165 France) which is commonly used to determine the phospholipid amount in serum. This colorimetric  
 166 enzymatic titration is based on the assay of the choline moiety of phospholipids. To do this, 10  $\mu$ L of  
 167 specimens or a standard solution were mixed with the reagent solutions provided by the BIOLABO  
 168 titration kit. The mixtures were stirred 10 min. at 37°C. Then, the absorbance at 500 nm of all samples  
 169 was measured. The DOPC concentration was finally calculated as Equation (2):

$$170 \quad \text{DOPC concentration} = \text{Standard concentration} \times \frac{\text{Abs(specimen)}}{\text{Abs(standard)}} \times 100 \quad (2)$$

### 171 **NPs concentration measurements by NP Tracking Analysis (NTA)**

172 The concentration of nanoMOFs modified with DOPC or PEG-lipid conjugates at different weight  
 173 ratios was investigated by Nanosight (LM10 Instrument, Malvern Instruments Ltd, Orsay, France),  
 174 which combines a conventional optical microscope with a laser to illuminate the NPs in Brownian  
 175 motion. Of main interest here, the size distribution and concentration could be determined  
 176 simultaneously. Results are expressed as means of five independent measurements.

### 177 **Colloid stability characterization by DLS**

178 The colloid stability of the nanoMOFs before and after lipid surface modification was monitored in  
 179 water every day during three weeks’ storage at 4°C. The stability in biological medium, including cell  
 180 culture medium and phosphate buffer saline (PBS) used in this study, was also measured at 0, 0.5, 1,  
 181 2, 4, 6, and 8 h after incubation at 37°C.

### 182 **Drug release and degradation of nanoMOFs**

183 Drug release was performed in PBS of different concentrations at 37°C. Briefly, drug loaded  
 184 nanoMOFs were centrifuged at 10,000 g for 10 min and the pellet was re-dispersed in 1mL water by  
 185 vortex. Aliquots of 100  $\mu$ L were taken and mixed with 900  $\mu$ l of the media used for release. The final

186 concentration of PBS was 1, 3, and 6 mM and nanoMOFs of 2.0 mg/mL. After different incubation  
187 times at 30 min, 1 h, 2 h, 4 h, 6 h and 24 h), the suspensions were centrifuged and the supernatants  
188 were assessed by HPLC as previously described to determine the amount of released drug. Moreover,  
189 the trimesate release was also evaluated by HPLC. Briefly, trimesate was analyzed with a mobile phase  
190 consisting of 90% buffer (5.75 g/L of  $\text{NH}_4\text{H}_2\text{PO}_4$ ): 10% Acetonitrile containing 5 mM TBAP. The  
191 injection volume was 5  $\mu\text{L}$  and the detection wavelength was set at 220 nm.

## 192 Human plasma protein adhesion tests

193 Human serum albumin (HSA) was used in this study. NanoMOFs modified or not (300  $\mu\text{g}/\text{mL}$ ) was  
194 incubated with HSA at 100  $\mu\text{g}/\text{mL}$  in 10mM phosphate buffer at 37°C. The samples were centrifuged  
195 at 10,000 g for 5 min to remove the nanoMOFs after 1, 2, 4, 6, 8 and 12 h incubation. The excessive  
196 amounts of HSA in the supernatant were quantified using a bicinchoninic acid (BCA) assay.

## 197 NanoMOF internalization in macrophage

198 NanoMOF internalization was quantified by Inductively Coupled Plasma Mass Spectrometry (ICP-  
199 MS). Macrophage cells (J774A.1) were seeded at a density of  $2.0 \times 10^5$  cells per well in 24-well plates.  
200 Cells were cultured in cell culture medium at 37°C in 5%  $\text{CO}_2$  overnight for attachment. Cells were  
201 then incubated with 1 mL cell culture media containing nanoMOFs coated or not with lipids (nanoMOF  
202 concentration = 50  $\mu\text{g}/\text{mL}$ ). At the end of the 4 h incubation, the cells were washed with PBS for three  
203 times to eliminate the excess of MOFs. Cells were finally dried and digested using aqua regia (15  
204 minutes under ultrasonic bath), Fe quantification was performed using an ICP-MS equipped with a  
205 triple quadrupole (Agilent 8800, Agilent Technologies, Japan). Fe and Co were added as internal  
206 standard on samples and calibration standards solution at a concentration of 10  $\mu\text{g}/\text{L}$ . Isotopes were  
207 detected using “on-mass mode” ( $^{54}\text{Fe}^+$ ,  $^{56}\text{Fe}^+$ ,  $^{59}\text{Co}^+$ ). Helium was introduced into the collision/reaction  
208 cell at a flow rate of 3 mL/min. Dwell time for each of the targeted isotopes was 1 s. Fe was quantified  
209 using external calibration prepared using certified 1000 mg/L Fe standard solution (Merck, Germany).  
210 Operation conditions were daily optimized using a tuning solution.

## 211 Cytotoxicity assessment

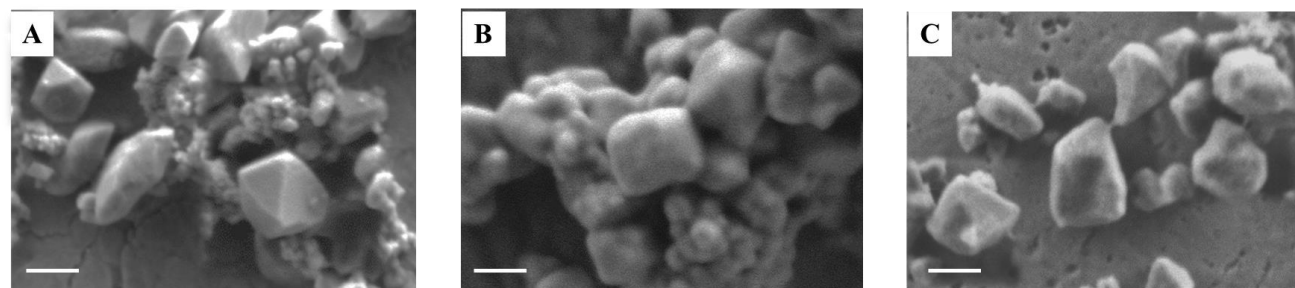
212 MTT assays were carried out on SKOV3 ovarian cancer cell line to investigate the cytotoxicity of NPs.  
213 The cells were plated in 96 well plates at a concentration of 10,000 cells per well. The media was  
214 removed after 24 h incubation and replaced by fresh media containing the MOFs nanoparticles at  
215 different concentrations. The cytotoxicity was assessed by MTT assay at 24, 48 and 72 h following the  
216 incubation of the cells with the MOFs. In brief, 100  $\mu\text{L}$  of complete media containing 0.5 mg/mL of  
217 MTT was added to cells and incubated for 2 h at 37°C in a 5%  $\text{CO}_2$  humidified atmosphere.  
218 Subsequently, the MTT media was removed and replaced by 100  $\mu\text{L}$  of DMSO per well to dissolve the  
219 MTT-formazan crystals. The plates were shaken for 10 min at 350 rpm in a Heidolph Titramax 101  
220 orbital shaker, and the absorbance at 595 nm was measured with the Tecan spark M10 plate reader.  
221 Each MTT experiment was reproduced three times.

## 222 RESULTS AND DISCUSSION

### 223 MIL-100 (Fe) nanoMOF surface modification and characterization of functionalized nanoMOFs

224 Iron trimesate nanoMOFs with mean diameters of  $232 \pm 14$  nm and Brunauer–Emmett–Teller (BET)  
225 surface areas of  $1519 \pm 50$   $\text{m}^2 \cdot \text{g}^{-1}$  were successfully synthesized by a “green” organic solvent-free  
226 hydrothermal method exempt of toxic additives such as hydrofluoric acid (Agostoni et al., 2013). They

227 were crystalline and exhibited a faceted morphology (**Figure 2A**) in agreement with previously  
 228 reported data (Cutrone et al., 2019b, 2019a).



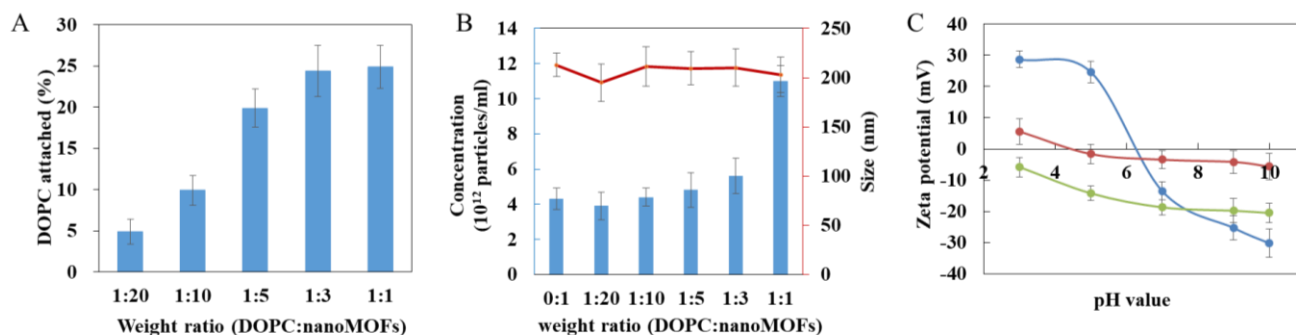
229  
 230 **Figure 2. Representative scanning electron microscope (SEM) images of nanoMOFs before and**  
 231 **after lipid modification.** (A) nanoMOFs; (B) nanoMOFs after modification with DOPC; (C)  
 232 nanoMOFs after modification with DOPC and DSPE-PEG 2000. Scale bar: 100  $\mu$ m.

233 In an attempt to achieve “stealth” NPs, the as-synthesized nanoMOF were surface functionalized with  
 234 PEG-lipid conjugates in a one-step procedure using a mixture of DSPE-PEG 2000 and DOPC. Lipids  
 235 were associated within less than 2 minutes at room temperature by dispersing the nanoMOFs in an  
 236 ethanolic aqueous solution containing both DSPE-PEG 2000 and DOPC, followed by a quick addition  
 237 of water to favor lipid deposition onto the nanoMOF surface. Indeed, lipids were freely soluble in  
 238 ethanol/water mixtures, but they readily precipitated upon progressive addition of water which  
 239 drastically reduced their solubility, leading to precipitation onto the nanoMOF surfaces (Wuttke et al.,  
 240 2015). DOPC-coated nanoMOFs were prepared as controls using the same method. The bare and  
 241 coated nanoMOFs were characterized by a set of complementary methods.

242 Firstly, SEM images show that the lipid-coated nanoMOFs displayed similar shapes but with more  
 243 rounded edges (Figure 2B) as compared to the uncoated ones (Figure 2A), possibly because surface  
 244 modification. No significant differences were observed for the coated nanoMOFs with or without PEG-  
 245 lipid conjugates (Figure 2C). Secondly, EDX experiments were performed to detect the presence of  
 246 elements specific to the MOF cores (C, O, Fe) and to the shells (C, O, N) in the top layers of the NPs  
 247 (around 10 nm depth). The presence of the DOPC coating was evidenced by the detection of an N peak  
 248 characteristic of DOPC which was not found with bare nanoMOFs (Figure S1). Interestingly, in the  
 249 PEG shells obtained with the lipid mixtures, the relative O content was increased by a factor of 4 as  
 250 compared to DOPC coatings (Figure S1) possibly due to the presence of PEG chains in the nanoMOFs’  
 251 top layers, as PEG has the highest O content from all the nanoMOF components. These data offer a  
 252 straightforward proof for both the presence of DOPC and PEG-lipid conjugates in the nanoMOF top  
 253 layers.

254 The amount of DOPC in the nanoMOFs was quantified by using a colorimetric enzymatic method. For  
 255 this, the DOPC:nanoMOF weight ratio in the preparation procedure was varied from 1:20 to 1:1. As  
 256 shown in Figure 3A, the amount of lipids associated to the nanoMOFs increased with the amount of  
 257 lipids used in the coating procedure. A plateau was reached at a DOPC: nanoMOF weight ratio of 1:3,  
 258 corresponding to  $25 \pm 4$  wt% lipids associated to the nanoMOFs. These quantities of coating material  
 259 are among the highest reported so far (Horcajada et al., 2010; Agostoni et al., 2015; Bellido et al., 2015;  
 260 Hidalgo et al., 2017; Giménez-marqués et al., 2018; Cutrone et al., 2019b, 2019a). As comparison,  
 261 phosphorylated cyclodextrin (CD-P) coatings on same iron trimesate nanoMOFs reached  $\sim 17$  wt%  
 262 (Agostoni et al., 2015). The important lipid association could be possibly due to: i) the fast precipitation

263 of lipids at the hydrophobic surface of nanoMOFs, and ii) the strong affinity of the phosphate groups  
 264 in the lipids for the iron sites at the nanoMOFs' surface.



265

266 **Figure 3. Characterization of lipid-coated nanoMOFs.** (A) Quantification of the amount of DOPC  
 267 in the nanoMOFs; (B) Mean hydrodynamic diameter (red) and concentration (blue) of DOPC-coated  
 268 nanoMOFs determined by NTA. (C) Zeta potential of nanoMOFs as a function of pH before (blue) and  
 269 after lipid coating with (red) or without (green) the addition of DSPE-PEG 2000.

270 The nanoMOFs, coated or not, were characterized by a set of complementary methods. First, X-ray  
 271 powder diffraction (XRPD) showed that the crystalline structure of the nanoMOFs was preserved after  
 272 surface modification (Figure S2). Dynamic light scattering (DLS) proved that there were no significant  
 273 differences between the mean hydrodynamic diameters of nanoMOFs before and after surface  
 274 functionalization ( $232 \pm 14$  nm,  $241 \pm 17$  nm and  $238 \pm 11$  nm for uncoated nanoMOFs, lipid coated  
 275 nanoMOFs at a DOPC: nanoMOF weight ratio of 1:3, with and without DSPE-PEG 2000,  
 276 respectively). Moreover, the BET surface areas were not affected by surface modification with lipids  
 277 ( $1519 \pm 50$  m<sup>2</sup>.g<sup>-1</sup>,  $1486 \pm 70$  m<sup>2</sup>.g<sup>-1</sup>, and  $1547 \pm 80$  m<sup>2</sup>.g<sup>-1</sup> for uncoated nanoMOFs, lipid coated  
 278 nanoMOFs with and without DSPE-PEG 2000, respectively), suggesting that the bulky lipids were  
 279 located onto the nanoMOF's external surfaces rather than into their porosity.

280 Before surface modification, the nanoMOF concentration was around  $(4 \pm 0.8) \times 10^{12}$  particles/mL, as  
 281 determined by Nanoparticle Tracking Analysis (NTA). Interestingly, the nanoMOF particle  
 282 concentration did not change upon modification with lipids (Figure 3B, blue histograms), suggesting  
 283 that the lipids adhered at their surface and did not remain into the suspension medium. Indeed, at  
 284 DOPC:nanoMOFs weight ratios from 0:1 up to 1:3, both particle concentrations and mean  
 285 hydrodynamic diameters were unaffected ( $(5.6 \pm 0.8) \times 10^{12}$  particles/mL, and  $210 \pm 23$  nm,  
 286 respectively). To support this hypothesis, DLS analysis of supernatants (Table S1) after particle  
 287 centrifugation revealed that they were devoid of any lipid vesicles (<1% particles free).

288 However, addition of excess lipids (weight DOPC:nanoMOF ratio of 1:1) resulted in a dramatic  
 289 increase of total particle concentration (from  $(4 \pm 0.8) \times 10^{12}$  to  $(1.1 \pm 0.4) \times 10^{13}$  particles/mL),  
 290 presumably because the nanoMOF surfaces were saturated with lipids. Of note, the mean  
 291 hydrodynamic diameter of the nanoMOFs was unaffected, only the polydispersity index (PdI)  
 292 increased from 0.15 to 0.25, possibly because of the presence of lipid vesicles in excess. Note that the  
 293 association of DSPE-PEG 2000 didn't significantly influence the mean hydrodynamic diameter, nor  
 294 the nanoMOF's concentration (less than 10% variations) suggesting that the PEGylated lipids also  
 295 associated onto the nanoMOFs. In conclusion, lipids were associated up to  $25 \pm 4$  wt% without  
 296 inducing any changes in nanoMOF porosities, size distribution, and crystallinity.

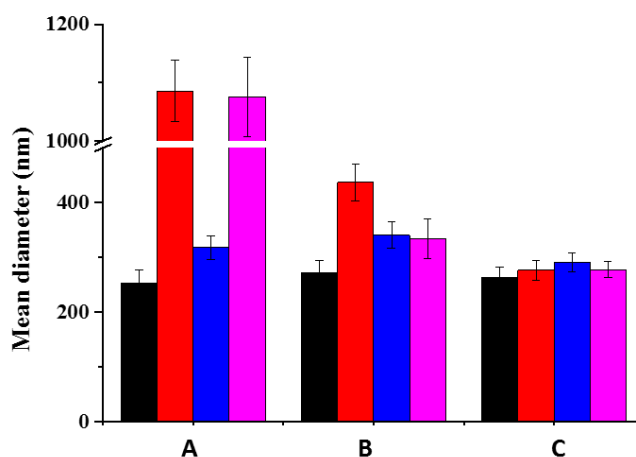
297 Interestingly, the presence of the coatings affected the nanoMOFs electrophoretic mobility, as shown  
298 by Zeta potential (ZP) investigations in Figure 3C. Indeed, the ZP of the uncoated nanoMOFs was  
299 strongly dependent upon the pH of the suspension medium, shifting from positive values ( $+23 \pm 3$  mV)  
300 at pH lower than 5 to negative values ( $-15 \pm 3$  mV) at basic pH. This could be probably due to the  
301 presence of both uncoordinated iron sites and terminal carboxyl groups of the trimesate ligands at the  
302 external nanoMOFs surface (Cutrone et al., 2019b). The ZP values were dramatically altered after  
303 surface modification (Figure 3C). DOPC-coated nanoMOFs displayed negative ZP values (-6 to -20  
304 mV) whatever the pH in the range of 3 to 10, in line with data reported for DOPC liposomes (Chibowski  
305 and Szcześ, 2016). These results support the presence of DOPC lipid layers onto the nanoMOFs which  
306 shield their charged surface moieties. Interestingly, when the nanoMOFs were surface-functionalized  
307 with PEG chains, their ZP values were shifted to neutral ( $-1.6 \pm 3.4$  mV). This is in good agreement  
308 with other studies on PEG-coated NPs (Gref et al., 1995; Thevenot et al., 2007; Troutier and Ladavière,  
309 2007; Troutier-Thuilliez et al., 2009; Bugnicourt et al., 2019).

### 310 **Effect of the coatings on the colloidal stability of nanoMOFs in biological media**

311 As the majority of uncoated NPs, nanoMOFs suffer from poor stability in biological media, which  
312 hampers their biomedical applications. Figure 4 clearly shows that uncoated nanoMOFs undergo a fast  
313 aggregation in both phosphate buffer saline (PBS, pH=7.4, 10 mM) and cell culture medium DMEM  
314 (Dulbecco's Modified Eagle Medium) without fetal bovine serum (FBS), with the mean hydrodynamic  
315 diameters rapidly increasing to more than 1  $\mu$ m within only 6 h at 37°C (Figure 4). No significant  
316 variation was observed for the mean hydrodynamic diameter of uncoated nanoMOFs in water in the  
317 first 1 h, however, they tended to aggregate upon storage (Figure S3). They were stable only in DMEM  
318 supplemented with 10% (v/v) FBS, possibly due to the formation of a protein corona at their surface  
319 preventing their aggregation (see section 2.5).

320 In contrast, DOPC coated nanoMOFs were stable both in water and DMEM. No aggregation was  
321 observed even after 3 weeks storage. However, they still underwent aggregation in PBS (Figure 4).  
322 Remarkably, PEGylation allowed circumventing stability issues, whatever the suspension media (less  
323 than 10% diameter variation in PBS).

324 As all the coated and uncoated nanoMOFs were stable in DMEM supplemented with 10% (v/v) FBS,  
325 it was possible to explore further their cytotoxicity and interactions with cancer cell lines and  
326 macrophages. The PEGylated nanoMOFs exhibited excellent colloidal stability in all the tested  
327 biological media and thus appeared as optimal candidates for biological applications.



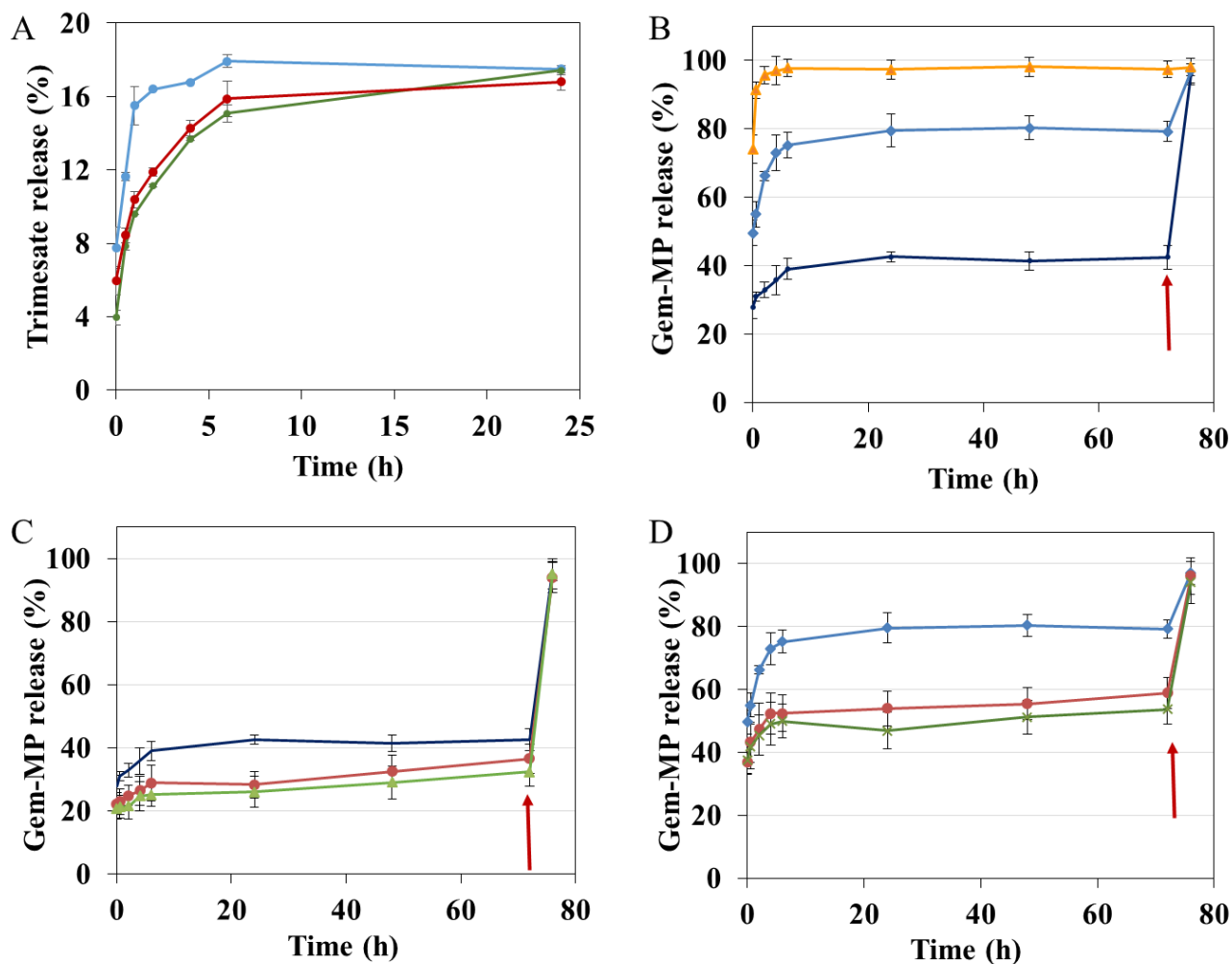
328

329 **Figure 4. Colloidal stability of nanoMOFs in different media, before (A) and after surface**  
 330 **functionalization with DOPC (B) or PEG-lipid conjugates (C).** Mean hydrodynamic diameters of  
 331 nanoMOF suspensions at 100  $\mu\text{g/mL}$  were determined by DLS after 6 h incubation at 37°C. (Black:  
 332 water; red: PBS; blue: DMEM supplemented with 10v/v% FBS; pink: DMEM without FBS).

### 333 Control of degradation and drug release by lipid coating

334 There is a general agreement on the fact that once the nanomaterials release their drug cargo, they  
 335 should degrade to avoid accumulation inside the body (Horcajada et al., 2012). However, Fe-based  
 336 nanoMOFs are reported to degrade rapidly in the biological media, because of coordination of various  
 337 ions (phosphates, sulfates, etc) to their iron sites, sometimes leading to uncontrolled “burst” drug  
 338 release (Agostoni et al., 2013; Li et al., 2017, 2019b). It was therefore interesting to investigate if the  
 339 hydrophobic lipid coatings could interfere with the rapid penetration of the aqueous degrading media  
 340 inside the pores, thus allowing gaining better control upon the release and degradation mechanisms.

341 Degradation of nanoMOFs is generally monitored by the release of the constituting ligand trimesate  
 342 (Agostoni et al., 2013; Rodriguez-Ruiz et al., 2015; Li et al., 2017). The degradation of the lipid-coated  
 343 or bare nanoMOFs was studied by assaying ligand trimesate by HPLC in PBS (Figure 5A). In PBS 1  
 344 mM, uncoated nanoMOFs (blue curve, Figure 5A) underwent a fast degradation in the first 1 h at 37°C  
 345 with around  $15.5 \pm 1.1$  % trimesate released, in agreement with previous reports (Li et al., 2017). It  
 346 was discovered that in the same conditions, the lipid-coated nanoMOFs, with (red curve, Figure 5A)  
 347 or without PEG-lipids conjugates (green curve, Figure 5A), exhibited much slower degradation profiles  
 348 than the uncoated nanoMOFs, with only  $10 \pm 0.2\%$  trimesate release in the first 1 h. This suggests a  
 349 more progressive diffusion of the phosphate ions into the coated nanoMOFs, slowing down their  
 350 degradation. However, the same plateau was reached after 24 h incubation, corresponding to a total  
 351 complexation of the phosphates in the medium (Li et al., 2017). In conclusion, the shell efficiently  
 352 delayed the degradation process.



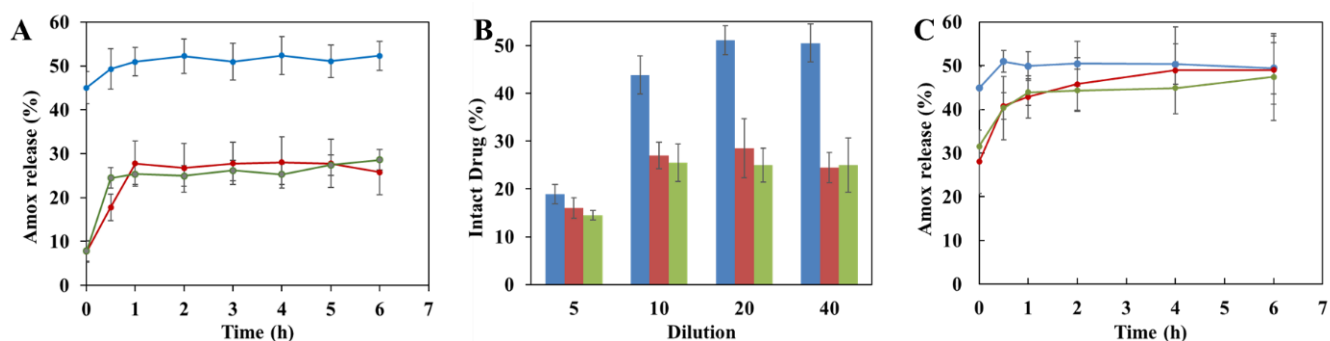
353  
 354 **Figure 5 Effect of surface modification on Gem-MP and trimesate release analyzed by HPLC.** A:  
 355 Trimesate release in 1mM PBS from nanoMOFs before (blue) and after lipid coating with (red) or  
 356 without (green) coating with PEG-lipid conjugates after incubation at 37 °C. B: Gem-MP release from  
 357 uncoated nanoMOFs in PBS with different molarities (orange: 6 mM, blue: 3 mM; dark blue: 1 mM).  
 358 Gem-MP release in 1 mM (C) or 3 mM (D) PBS from nanoMOFs before (blue/dark blue) and after  
 359 lipid coating with (red) or without (green) coating with PEG-lipid conjugates. In all cases (B, C, and  
 360 D), phosphate concentration was adjusted to 10 mM after 72 h incubation at 37°C (red arrows),  
 361 followed by further incubation for 4 h at 37°C.

362 Then, the effect of lipid coatings on drug release was studied. Selected drug of interest was Gem-MP,  
 363 a hydrophilic drug with low penetration inside cancer cells. NanoMOFs acted as efficient  
 364 "nanosponges", soaking Gem-MP from their aqueous solution with almost perfect efficiency (>98%).  
 365 Maximal loadings reached 25 wt% reflecting the strong interaction between the drug and the iron  
 366 trimesate matrices. Advantageously, the lipid coating didn't induce any significant drug release during  
 367 the coating procedure (less than 3% variations before and after coating).

368 Gem-MP release is governed by a competition of coordination between the phosphate moieties in Gem-  
 369 MP and free phosphates in PBS for the iron(III) Lewis acids of nanoMOFs (Agostoni et al., 2013,  
 370 2015; Rodriguez-Ruiz et al., 2015). As expected, it was found that the higher the amount of phosphates,  
 371 the higher the amount of drug released (Figure 5B). At low phosphate concentrations (PBS 1 mM or 3

372 mM), a plateau (around 40% or 80% Gem-MP release) was reached in 24 h, when all the phosphate  
 373 molecules present in the release medium were complexed to the iron sites, as previously reported  
 374 (Agostoni et al., 2013, 2015; Rodriguez-Ruiz et al., 2015). When additional phosphates were added in  
 375 the release medium, all the drug still remaining in the nanoMOFs was immediately released (Figure  
 376 5B, arrow). Gem-MP release was well correlated with particle degradation, resulting in trimesate  
 377 release (Figure S4).

378 The presence of the lipid coating reduced the drug release from the nanoMOFs (Figure 5C). For  
 379 instance, after 6 h incubation in PBS 1 mM, around 30% Gm-MP was released from the coated  
 380 nanoMOFs, in comparison to 40% with the uncoated ones. This is possibly due to the restricted  
 381 diffusion of phosphates into the nanoMOFs because of the lipid coating. Similarly, after 6 h incubation  
 382 in PBS 3 mM, around 50% Gem-MP was released from the coated nanoMOFs, in comparison to 78%  
 383 with the uncoated ones (Figure 5D). The Gem-MP release from coated nanoMOFs gradually increased  
 384 in a sustained manner in the following days (Figures 5C, D). All the remained drugs could be released  
 385 out after 4 h incubation in concentrated phosphate buffer (10 mM PBS).



386 **Figure 6.** Effect of coating on Amox release in water (A, B) and in PBS (C). A: Release kinetics of  
 387 Amox in water from nanoMOFs (1mg/mL) before or after coating, with a dilution factor of 20; B:  
 388 Effect of dilution factor on Amox release after 4 h incubation at 37°C in water; (Blue: uncoated  
 389 nanoMOFs; red: DOPC coated nanoMOFs; Green: DOPC and PEG-lipid conjugate coated nanoMOFs)  
 390

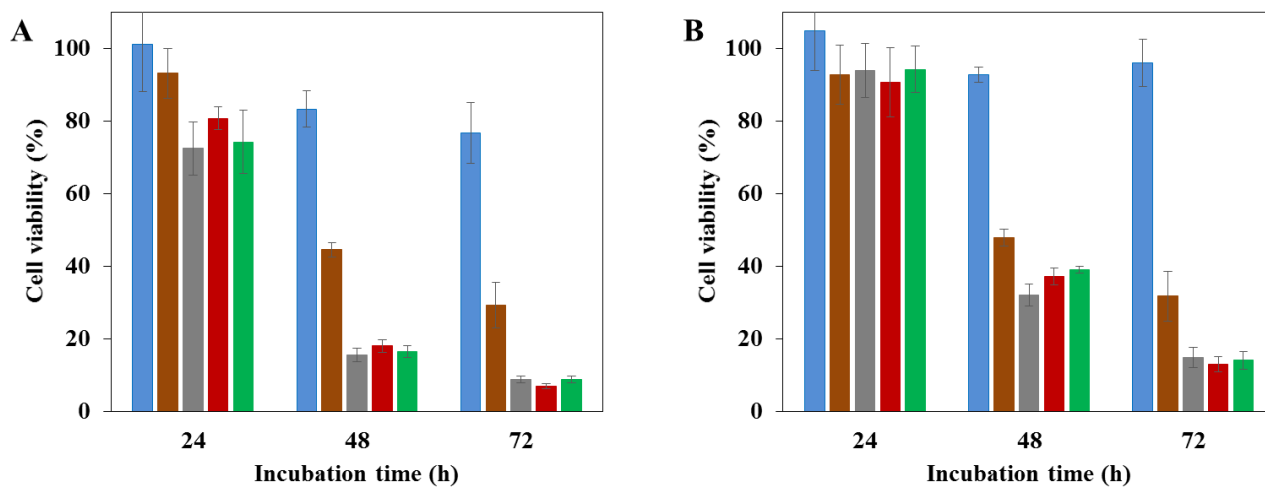
391 Similar results were found with another drug, amoxicillin (Amox). The amount of Amox released in  
 392 the first hour of incubation release was reduced by a factor of two in the case of lipid-coated nanoMOFs  
 393 as compared to the naked ones (Figure 6A). However, in the presence of strongly complexing  
 394 phosphates, the degradation was only delayed, but not avoided (Figure 6C).

### 395 Cytotoxicity assays of nanoMOFs on ovarian cancer cells

396 All the studied nanoMOFs were nontoxic for the SKOV3 ovarian cancer cells up to 100  $\mu\text{g/mL}$  (Figure  
 397 7A, blue histograms), with more than 98% cell viability in 24 h, which is in agreement with previously  
 398 reported lack of toxicity of these materials (Horcajada et al., 2010; Baati et al., 2013; Bellido et al.,  
 399 2015; Giménez-marqués et al., 2018; Li et al., 2019b). In contrast, as expected, the anticancer drug  
 400 Gem-MP (20  $\mu\text{g/mL}$ , Figure 7A, brown histograms) exerted a cytotoxic effect with 45% cell viability  
 401 after 48 h incubation, which further diminished to 29% in 72 h. Remarkably, Gem-MP loaded  
 402 nanoMOFs showed a strong *in vitro* activity on SKOV3 ovarian cancer cells, higher than the free drug  
 403 (Figure 7). At equivalent Gem-MP concentrations, whatever the drug loading (8 or 20 wt%) and the  
 404 amount of nanoMOF in contact with the cells (10 to 100  $\mu\text{g/mL}$ ), the drug-loaded nanoMOFs  
 405 outperformed the free drug in terms of toxicity on cancer cells (Figure 7 and Figure S5).

406 This is in line with previous studies showing the efficient internalization on nanoMOFs in cancer cells  
 407 (Rodriguez-Ruiz et al., 2015; Li et al., 2019a). It was recently shown that nanoMOFs acted as “Trojan

408 horses” by internalizing inside the cancer cells, carrying their Gem-MP cargo to interfere with DNA  
 409 (Li et al., 2019a). In this study it was shown that interestingly, the presence of a lipid coating  
 410 (PEGylated or not) did not reduce the nanoMOF anticancer efficacy on SKOV3 ovarian cancer cells.



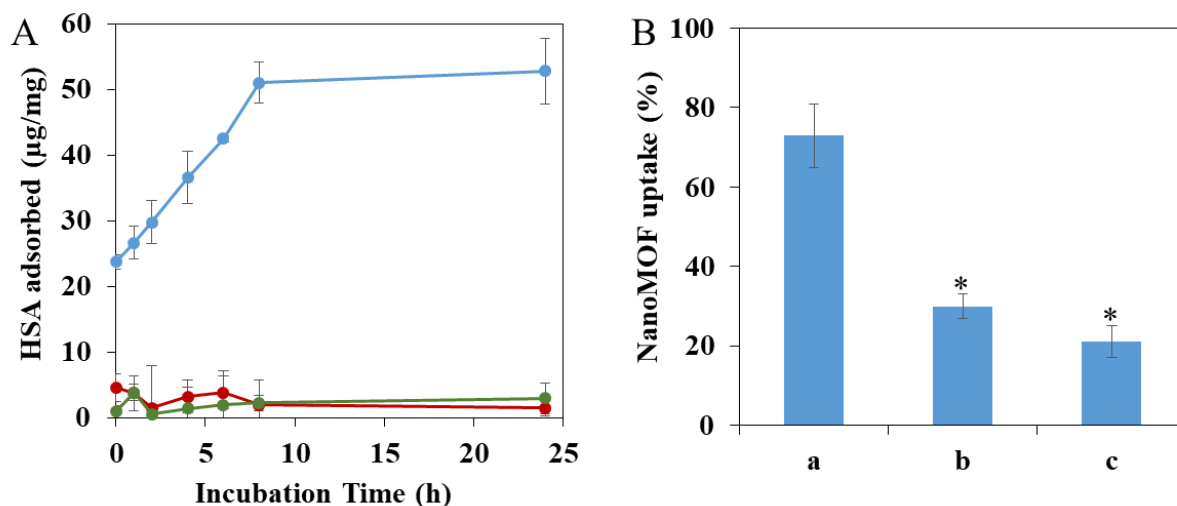
411

412 **Figure 7 Cytotoxicity measured by MTT assays of nanoMOFs (blue), anticancer efficacy of Gem-**  
 413 **MP (brown), Gem-MP loaded nanoMOFs before (grey) and after coating with DOPC (red) or**  
 414 **PEG-lipid conjugates (green).** The experiments were performed on SKOV3 ovarian cancer cells, at  
 415 different incubation times, with different concentrations nanoMOFs. A: 100µg/mL; B: 30µg/mL. Gem-  
 416 MP loading was 20 wt%.

417 **Effect of surface functionalization of nanoMOFs on protein adsorption and macrophage uptake**

418 It is well known that intravenously administered NPs are readily covered by plasma proteins, creating  
 419 the so-called “protein corona”, which plays a crucial role on the NPs’ biodistribution and *in vivo* fate  
 420 (Gref et al., 2000). To gain insight on the influence of lipid coating of nanoMOFs on protein adsorption,  
 421 HSA (human serum albumin), the most abundant protein in human blood plasma, was selected for this  
 422 study.

423 NanoMOFs coated or not with DOPC lipids and PEG-lipid conjugates were incubated for 4 h at 37°C  
 424 with HSA. After separation of the supernatants by centrifugation, the amount of non-adsorbed HSA  
 425 was quantified thanks to a BCA titration in order to indirectly determine the adsorbed HSA amounts  
 426 onto nanoMOFs, lipid-modified or not. These amounts, expressed as µg/mg of nanoMOFs, are reported  
 427 in Figure 8A. In the case of uncoated nanoMOFs (Figure 8A, blue curve), the amount of adsorbed HSA  
 428 reached a plateau within 6 h, with around 50 µg HSA/mg nanoMOFs. Interestingly, lipid coating  
 429 dramatically reduced HSA adsorption, with ~5 µg HSA/mg nanoMOFs (Figure 8A, green curve),  
 430 regardless of the addition of DSPE-PEG 2000 (Figure 8A, red curve). To the best of our knowledge,  
 431 the adsorbed HSA amounts are among the lowest reported with MIL-100 (Fe) nanoMOFs (Gref et al.,  
 432 2000; Cutrone et al., 2019b). These results suggest that lipid-based coating on nanoMOFs is efficient  
 433 to avoid albumin adsorption.



434

435 **Figure 8 HSA adsorption assayed by BCA assay (A) and J774 murine macrophage uptake (B) of**  
 436 **nanoMOFs before and after lipid surface functionalization.** A: HSA adsorption by nanoMOFs  
 437 before (blue) and after lipid coating with (red) or without (green) the addition of DSPE-PEG 2000. B:  
 438 NanoMOFs (before and after lipid coating, with or without addition of DSPE-PEG 2000)  
 439 internalization inside murine macrophage J774 cells. 50 µg/mL nanoMOFs were incubated with  $3 \times 10^5$   
 440 J774 cells for 4 h, and the amount of internalized nanoMOFs was determined by ICP-MS and expressed  
 441 as a % of the initial nanoMOF amount in contact with the cells. **Significant difference was observed**  
 442 **for nanoMOFs before and after surface modification ( $p < 0.01$ ).**

443 The potential “stealth” effect of the lipid-coated nanoMOFs, PEGylated or not, was evaluated on the  
 444 murine macrophage cell line J774. Quantitative data on the amounts of nanoMOFs internalized in cells  
 445 were obtained by ICP-MS, after extensive washing to remove the non-associated particles. An  
 446 incubation time of 4 h was chosen as it corresponds to the typical blood circulation time of PEG-coated  
 447 NPs (Cutrone et al., 2019b). Interestingly, the DOPC coating of nanoMOFs reduced their macrophage  
 448 uptake by a factor of 2.4, from  $75 \pm 6\%$  to  $31 \pm 3\%$ . The nanoMOF functionalization with PEG chains  
 449 was even more effective, reducing their interactions with macrophage to  $21 \pm 2\%$ . **However, it is widely**  
 450 **known that numerous complex interactions can occur after NP administration in multicellular**  
 451 **organisms. Therefore, in vivo studies need to be carried on to demonstrate the efficacy of the PEG**  
 452 **coating to reduce reticuloendothelial system (RES) uptake.**

453 For the sake of comparison, in similar experimental conditions, other coating materials showed higher  
 454 interactions with macrophages, for instance,  $41 \pm 3\%$  for CD-P coating, and  $39 \sim 24\%$  for comb-like  
 455 copolymers (Cutrone et al., 2019a, 2019b). The advantage of lipid coating, demonstrated in this work,  
 456 is a straightforward method, leading to efficient and stable coatings based on already FDA-approved  
 457 materials.

## 458 CONCLUSION

459 The surface of iron trimesate nanoMOFs was successfully modified with FDA approved DSPE-PEG  
 460 2000 in combination with DOPC by a fast solvent-exchange deposition method. We described herein  
 461 the preparation and comprehensive characterization of the lipid modified NPs. For the first time, we

462 showed that the lipid surface modification of porous nanoMOFs reduced both their tendency to degrade  
463 rapidly in PBS. Moreover, the coating of nanoMOFs with PEG-lipid conjugates successfully decreased  
464 their uptake by macrophages *in vitro* by a factor of 3.6. Moreover, nanoMOFs acted as “Trojan horses”  
465 internalizing inside the cancer cells, and carrying their Gem-MP cargo to interfere with DNA.

#### 466 DATA AVAILABILITY STATEMENT

467 The datasets generated for this study are available on request to the corresponding author.

#### 468 AUTHOR CONTRIBUTIONS

469 RG conceived the study. RG, XL and GS designed the experiments. XL, GS, and JQ performed the  
470 experiments. CL contributed to the lipid investigations. XL and RG wrote the manuscript. MM, KB  
471 and TT contributed to the biological evaluations. All authors approved the submitted version.

#### 472 CONFLICT OF INTEREST

473 The authors declare that the research was conducted in the absence of any commercial or financial  
474 relationships that could be construed as a potential conflict of interest.

#### 475 FUNDING

476 Financial support for this work was provided the French National Research Agency (ANR-14-CE08-  
477 0017 and ANR-16-CE18-0018) and EuroNanoMed3 PCInano. This work was also supported by a  
478 public grant overseen by the French National Research Agency as part of the “Investissements  
479 d’Avenir” program (Labex NanoSaclay, ANR-10-LABX-0035).

#### 480 ACKNOWLEDGMENTS

481 We acknowledge Dr. B. Moreira-Alvarez and Dr. J. R. Encinar for their kind help with ICP-MS  
482 analysis. We thank Dr. D. Constantin for help with XRPD experiments.

#### 483 SUPPLEMENTARY MATERIAL

484 The Supplementary Material for this article can be found online at:

#### 485 REFERENCES

- 486 Agostoni, V., Chalati, T., Horcajada, P., Willaime, H., Anand, R., Semiramo, N., et al. (2013).  
487 Towards an improved anti-HIV activity of NRTI via Metal-Organic Frameworks nanoparticles.  
488 *Adv. Healthc. Mater.* 2, 1630–1637.
- 489 Agostoni, V., Horcajada, P., Noiray, M., Malanga, M., Aykaç, A., Jicsinszky, L., et al. (2015). A  
490 “green” strategy to construct non-covalent, stable and bioactive coatings on porous MOF  
491 nanoparticles. *Sci. Rep.* 5, 7925.
- 492 Aykac, A., Noiray, M., Malanga, M., Agostoni, V., Casas-Solvas, J. M., Fenyvesi, E., et al. (2017). A  
493 non-covalent “click chemistry” strategy to efficiently coat highly porous MOF nanoparticles with  
494 a stable polymeric shell. *BBA - Gen. Subj.* 1861, 1606–1616.
- 495 Baati, T., Njim, L., Neffati, F., Kerkeni, A., Bouttemi, M., Gref, R., et al. (2013). In depth analysis of

- 496 the in vivo toxicity of nanoparticles of porous iron(III) metal-organic frameworks. *Chem. Sci.* 4,  
497 1597–1607.
- 498 Barenholz, Y. (2012). Doxil® - The first FDA-approved nano-drug: lessons learned. *J. Control.*  
499 *Release* 160, 117–134.
- 500 Bellido, E., Hidalgo, T., Lozano, M. V., Guillevic, M., Simón-Vázquez, R., Santander-Ortega, M. J.,  
501 et al. (2015). Heparin-engineered mesoporous iron Metal-Organic Framework nanoparticles:  
502 toward stealth drug nanocarriers. *Adv. Healthc. Mater.* 4, 1246–1257.
- 503 Bouffard, D. Y., Laliberté, J., and Momparler, R. L. (1993). Kinetic studies on 2',2'-  
504 difluorodeoxycytidine (gemcitabine) with purified human deoxycytidine kinase and cytidine  
505 deaminase. *Biochem. Pharmacol.* 45, 1857–1861.
- 506 Bugnicourt, L., Peers, S., Dalverny, C., and Ladavière, C. (2019). Tunable morphology of  
507 lipid/chitosan particle assemblies. *J. Colloid Interface Sci.* 534, 105–109.
- 508 Chibowski, E., and Szcześ, A. (2016). Zeta potential and surface charge of DPPC and DOPC liposomes  
509 in the presence of PLC enzyme. *Adsorption* 22, 755–765.
- 510 Cutrone, G., Li, X., Casas-Solvas, J. M., Menendez-Miranda, M., Qiu, J., Benkovics, G., et al. (2019a).  
511 Design of engineered cyclodextrin derivatives for spontaneous coating of highly porous Metal-  
512 Organic Framework nanoparticles in aqueous media. *Nanomaterials* 9, 1–26.
- 513 Cutrone, G., Qiu, J., Menendez-Miranda, M., Casas-Solvas, J. M., Aykaç, A., Li, X., et al. (2019b).  
514 Comb-like dextran copolymers: A versatile strategy to coat highly porous MOF nanoparticles  
515 with a PEG shell. *Carbohydr. Polym.* 223, 115085.
- 516 Giménez-marqués, M., Bellido, E., Berthelot, T., Simón-yarza, T., Hidalgo, T., Simón-vázquez, R., et  
517 al. (2018). GraftFast surface engineering to improve MOF nanoparticles furtiveness. *small* 14, 1–  
518 11.
- 519 Gref, R., Domb, A., Quellec, P., Blunk, T., Müller, R. H., Verbavatz, J. M., et al. (1995). The controlled  
520 intravenous delivery of drugs using PEG-coated sterically stabilized nanospheres. *Adv. Drug*  
521 *Deliv. Rev.* 16, 215–233.
- 522 Gref, R., Lück, M., Quellec, P., Marchand, M., Dellacherie, E., Harnisch, S., et al. (2000). “Stealth”  
523 corona-core nanoparticles surface modified by polyethylene glycol (PEG): Influences of the  
524 corona (PEG chain length and surface density) and of the core composition on phagocytic uptake  
525 and plasma protein adsorption. *Colloids Surfaces B Biointerfaces* 18, 301–313.
- 526 Gref, R., Minamitake, Y., Peracchia, M. T., Trubetskoy, V., Torchilin, V., and Langer, R. (1994).  
527 Biodegradable long-circulating polymeric nanospheres. *Science (80-. )*. 263, 1600–1603.
- 528 He, C., Liu, D., and Lin, W. (2015). Nanomedicine applications of hybrid nanomaterials built from  
529 Metal-Ligand Coordination bonds: Nanoscale Metal-Organic Frameworks and Nanoscale  
530 Coordination Polymers. *Chem. Rev.* 115, 11079–11108.
- 531 Hidalgo, T., Bellido, E., Avila, J., Asensio, M. C., and Salles, F. (2017). Chitosan-coated mesoporous  
532 MIL-100 (Fe) nanoparticles as improved bio-compatible oral nanocarriers. *Sci. Rep.* 100, 1–14.

- 533 Horcajada, P., Chalati, T., Serre, C., Gillet, B., Sebrie, C., Baati, T., et al. (2010). Porous Metal-  
534 Organic-Framework nanoscale carriers as a potential platform for drug delivery and imaging. *Nat.*  
535 *Mater.* 9, 172–178.
- 536 Horcajada, P., Gref, R., Baati, T., Allan, P. K., Maurin, G., and Couvreur, P. (2012). Metal-Organic  
537 Frameworks in biomedicine. *Chem. Rev.* 112, 1232–1268.
- 538 Li, X., Lachmanski, L., Safi, S., Sene, S., Serre, C., Grenèche, J. M., et al. (2017). New insights into  
539 the degradation mechanism of Metal-Organic Frameworks drug carriers. *Sci. Rep.* 7, 1–17.
- 540 Li, X., Porcel, E., Menendez-Miranda, M., Qiu, J., Yang, X., Pastor, A., et al. (2019a). Highly porous  
541 hybrid metal-organic nanoparticles loaded with gemcitabine-monophosphate: a multimodal  
542 approach to improve chemo and radiotherapy. *ChemMedChem* 15, 274–283.
- 543 Li, X., Semiramoth, N., Hall, S., Tafani, V., Josse, J., Laurent, F., et al. (2019b). Compartmentalized  
544 encapsulation of two antibiotics in porous nanoparticles: an efficient strategy to treat intracellular  
545 infections. *Part. Part. Syst. Charact.* 36, 1–9.
- 546 Rodriguez-Ruiz, V., Maksimenko, A., Anand, R., Monti, S., Agostoni, V., Couvreur, P., et al. (2015).  
547 Efficient “green” encapsulation of a highly hydrophilic anticancer drug in Metal-Organic  
548 Framework nanoparticles. *J. Drug Target.* 23, 759–767.
- 549 Rojas, S., Arenas-Vivo, A., and Horcajada, P. (2019). Metal-Organic Frameworks: A novel platform  
550 for combined advanced therapies. *Coord. Chem. Rev.* 388, 202–226.
- 551 Rosenblum, D., Joshi, N., Tao, W., Karp, J. M., and Peer, D. (2018). Progress and challenges towards  
552 targeted delivery of cancer therapeutics. *Nat. Commun.* 9, 1–12.
- 553 Senapati, S., Mahanta, A. K., Kumar, S., and Maiti, P. (2018). Controlled drug delivery vehicles for  
554 cancer treatment and their performance. *Signal Transduct. Target. Ther.* 3, 1–19.
- 555 Simon-Yarza, M. T., Baati, T., Paci, A., Lesueur, L. L., Seck, A., Chiper, M., et al. (2016).  
556 Antineoplastic busulfan encapsulated in Metal Organic Framework nanocarrier: first in vivo  
557 results. *J. Mater. Chem. B* 4, 585–588.
- 558 Taylor-Pashow, K. M. L., Della Rocca, J., Xie, Z., Tran, S., and Lin, W. (2009). Postsynthetic  
559 modifications of iron-carboxylate nanoscale Metal-Organic Frameworks for imaging and drug  
560 delivery. *J. Am. Chem. Soc.* 131, 14261–14263.
- 561 Thevenot, J., Troutier, A., David, L., Delair, T., and Ladavière, C. (2007). Steric stabilization of  
562 lipid/polymer particle assemblies by poly (ethylene glycol)-lipids. *Biomacromolecules* 8, 3651–  
563 3660.
- 564 Troutier-Thuilliez, A.L., Thevenot, J., Delair, T., and Ladavière, C. (2009). Adsorption of plasmid  
565 DNA onto lipid/polymer particle assemblies. *Soft Matter* 5, 4739–4747.
- 566 Troutier, A., and Ladavière, C. (2007). An overview of lipid membrane supported by colloidal  
567 particles. *Adv. Colloid Interface Sci.* 133, 1–21.
- 568 Wuttke, S., Braig, S., Preiß, T., Zimpel, A., Sicklinger, J., Bellomo, C., et al. (2015). MOF

569 nanoparticles coated by lipid bilayers and their uptake by cancer cells. *Chem. Commun.* 51,  
570 15752–15755.